Hindawi
Advances in Materials Science and Engineering
Volume 2020, Article ID 4314253, 14 pages
https://doi.org/10.1155/2020/4314253

Research Article

Studying Bump at Bridge Approach of Short Subgrade with Oblique Prestressed Concrete Overlaying Asphalt Layer

Fuqiang Liu,[1] Mulian Zheng,[1] Tao Wang,[2] Shuai Wang,[3] and Linlin Zhu[1]

[1]*Key Laboratory of Highway Engineering in Special Region, Ministry of Education, Chang'an University, South Erhuan Middle Section, Xi'an 710064, China*
[2]*School of Civil Engineering, Beijing Jiaotong University, Beijing 100044, China*
[3]*CCCC Highway Consultants Co., Ltd, Block A, Desheng International Center, 85 Dewai Street, Xicheng District, Beijing 100032, China*

Correspondence should be addressed to Mulian Zheng; zhengml@chd.edu.cn

Received 28 May 2020; Revised 31 July 2020; Accepted 12 September 2020; Published 22 September 2020

Academic Editor: Aboelkasim Diab

The differential settlement of short subgrade between two highway structures (bridges, tunnels, culverts, etc.) is significantly greater than that of the other subgrade for the insufficient compaction of short subgrade owing to limited construction site. This paper aims to establish the control criteria to prevent bump at bridge approach for differential settlement of short subgrade with oblique prestressed concrete overlying asphalt layer (AC + OPC) composite pavement. In this work, the short subgrade and AC + OPC composite pavement were defined. Meanwhile, the driving comfort was analysed and the control criteria for differential settlement of short subgrade with different lengths were obtained based on the driving comfort using the driving comfort test. Finally, the effects of different layer parameters on stress and deflection were investigated and the control criteria for differential settlement of short subgrade were established based on the void area beneath the slab using the finite element software ANSYS. Results show that the length of short subgrade between two highway structures is defined to be less than 200 m. The vehicle speed and longitudinal slope have significant effects on the vertical acceleration. The asphalt layer modulus, OPC layer thickness and modulus, base layer thickness and modulus, and foundation modulus have effects on the flexural stress and deflection, especially the OPC layer thickness. The relationship between the additional stress and void area beneath the slab is derived. In addition, the control criteria for differential settlement of short subgrade with different lengths are put forward based on the void area beneath the slab and driving comfort. The application of AC + OPC composite pavement can prevent bump at bridge approach of short subgrade effectively. The results of this paper can provide guidance for the application of AC + OPC composite pavement.

1. Introduction

Highways built in hilly or mountainous areas have many structures (bridges, tunnels, culverts, etc.) for the limitation of terrain and requirements of linear design. The short subgrade is often sandwiched between structures. The differential settlements between the short subgrade and structures are significantly greater than that of the other subgrade for the insufficient compaction of short subgrade owing to limited construction site. The differential settlement has great influences on the driving comfort and safety. In addition, it can aggravate the damage to vehicles and roads [1–4]. Actually, the human comfort has often been neglected by most previous studies [5–9]. The definition of short subgrade is still vague. While the research works on differential settlement of railway, composite structures and preventing bump at bridge approach have been done by many scholars.

Cao and Qu have studied the influence of subgrade differential settlement on riding performance of high-speed train [10]. Paixão et al. investigated the effect of differential settlement on the dynamic response of the train-track system [11]. Nielsen and Li studied the railway track geometry degradation due to differential settlement of ballast/

subgrade numerical prediction by an iterative procedure [12]. Jiang et al. studied the geometry mapping and additional stresses of ballastless track structure caused by subgrade differential settlement under self-weight loads in high-speed railways [13]. Guo and Zhai have made a long-term prediction of track geometry degradation in high-speed vehicle ballastless track system due to subgrade differential settlement [14]. Rith et al. have studied the behavior of RCC (roller compacted concrete)-base composite pavement at heavy duty area [15, 16]. Luther carried out a mechanistic investigation of reflection cracking of asphalt overlays [17]. McCullough studied the performance of continuously reinforced concrete pavement using three-dimensional nonlinear finite element model [18]. Robison and Luna analysed the stress of composite structures of slab and subgrade using the finite element model [19]. Chew et al. proposed that the cement piles were an effective and simple method to solve the bump at bridge approach [20]. Shi et al. built the finite element model and analysed the dissociation phenomenon between the slab and lower foundation [21]. Yu put the slab on the top of the subgrade through the bench back leg, which could reduce the impact of dynamic load on the slab [22]. Wang proposed to cancel the pillow beam below the free end of slab. Instead, he set a transition layer of two-gray-stabilized gravel with a certain length and thickness, which had good performances in practice [23]. Ding put forward the design method of slab size and tail pillow beam. He pointed out that the slab bearing capacity must meet the requirements to avoid the danger of sudden fracture caused by the serious void beneath slab [24]. Meanwhile, the use of slab usually cannot meet the requirements for the differential settlement of short subgrade is much greater than that of the other subgrade. Therefore, the AC + OPC composite pavement is proposed to solve the differential settlement of short subgrade. The AC + OPC composite pavement is a long-life pavement structure, which can combine the advantages of rigid and flexible pavement and make good use of its advantages in durability and bearing heavy load. In addition, the AC + OPC composite pavement has the characteristics of no compaction and setting seams in large length and so on. However, the control criteria for differential settlement of short subgrade with AC + OPC composite pavement have not been seen in related research works. In order to prevent bump at bridge approach of short subgrade, the control criteria are put forward based on the driving comfort and void area beneath slab.

The differential settlement is the common phenomenon at short subgrade. It has effects on the driving comfort and void beneath slab. Because the short subgrade is in different lengths, the effects of differential settlement on the driving comfort and void beneath slab are different. The additional stress will occur beneath the void slab and it can lead to the slab fracture. However, the AC + OPC composite pavement can overcome the problems induced by the differential settlement significantly. Therefore, the paper is conducted to obtain the control criteria for differential settlement of short subgrade in different lengths with AC + OPC composite pavement based on the driving comfort and void area beneath slab.

2. Definition of Short Subgrade and AC + OPC Composite Pavement

2.1. Definition of Short Subgrade. There is no clear definition of short subgrade. In China, the Ministry of Railways stipulated that it is better to prefer bridge to subgrade when the subgrade length is less than 150 m in the bridge-dense areas of I-class railway [25]. In other countries, few studies have been conducted on the short subgrade. The methods of strengthening subgrade, increasing stiffness, and reducing settlement were used to reduce the differential settlement of short subgrade. The composite pavement was recommended in the short subgrade (less than 200~300 m) by the Department of Transport of Shaanxi Province [26].

The geological conditions are relatively complex at the site of short subgrade. Due to the complex terrain and geological conditions, the curve sections are inevitable. The linearity is the shape of road surface, and it includes straight line, circular curve, and easement curve. When the combination failure of linearity appears at some places, the vehicle speed changes frequently and the driver's overstress causes the rapid acceleration of heart rate when the vehicle passes through those places. The relationship of speed and linearity is shown in Figure 1 [27].

The human mentality and physiology can interfere with vehicle vibration, thus affecting the driver's judgment. The driving comfort is influenced by the driving speed, linearity, and pavement roughness. Pan [27] studied the formation of psychological and physiological burden through the change of driver's pulse rate and blood pressure. The evaluation indicators of the driver's psychological and physiological burden were established using experimental and mathematical methods. The research work showed that the driver could relieve the overstress and discomfort effectively when the vibration time was more than 10 s. At present, special sections such as bridges of expressway generally limit the speed from 60 to 80 km/h, and the distance between two structures within 10 s at this speed is 166–220 m. It can be known that the impact on the comfort will be reduced when the subgrade length between two structures is more than 220 m.

It also can be known that the long transition section should be set up to reduce the adverse effects caused by the differential settlement of short subgrade on the comfort. Considering the relevant regulations of the Department of Transport of Shaanxi Province and the Ministry of Railways and the other related research results, the subgrade is defined as short subgrade when its length between two highway structures is less than 200 m.

2.2. AC + OPC Composite Pavement. The AC + OPC composite pavement is the composite structure of oblique prestressed concrete overlying asphalt layer. It is a kind of long-life pavement structure with combined advantages of rigid pavement and flexible pavement. The OPC layer of AC + OPC composite pavement is equipped with double oblique prestressed tendons. The prestressed tendons form a certain angle with the longitudinal structure. The realization

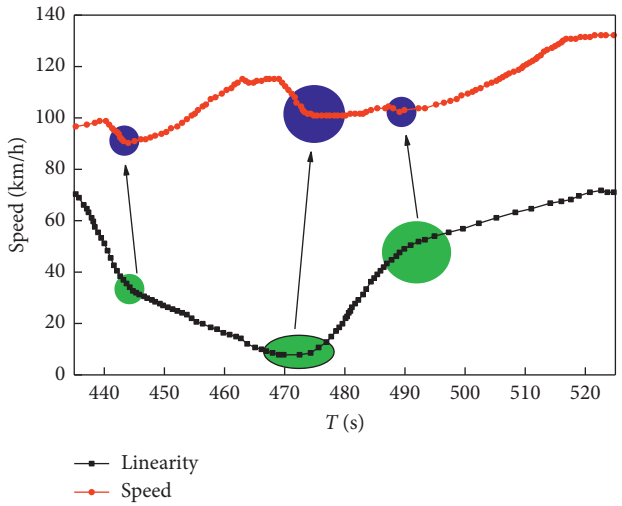

Figure 1: Relationship of speed and linearity.

of not setting seams in large lengths can solve the distresses of ordinary concrete pavement caused by seams and improve the pavement performance and life [28]. The OPC schematic diagram is shown in Figure 2.

The OPC structure has the following advantages compared with the other semirigid bases such as the two-gray-stabilized gravel and cement-stabilized gravel:

(1) It does not need compaction. It can reduce the differential settlement and deformation caused by insufficient compaction and the damage caused by the uneven load.

(2) It has good durability and high bearing capacity [29]. Therefore, it can replace the semirigid base as the main load-bearing layer.

(3) It can be connected with bridges and other structures at both ends of the subgrade, similar to a "slab."

(4) It can effectively prevent water from infiltrating into the subgrade through the seam.

In addition, the problem of reflecting cracks that usually appear in ordinary cement concrete overlying asphalt layer does not occur in AC + OPC composite pavement.

3. Testing Programme and Model Building

3.1. Testing Vehicle and Acceleration Sensor

3.1.1. Human Comfort and Testing Vehicle. Zheng used the vehicle vibration comfort to evaluate the comfort. The research was focused on the impacts of different measuring positions and different speeds on the vehicle comfort [30]. ISO2631 took the weighted acceleration mean square root value as the evaluation index of driving comfort and found the relationship between the weighted acceleration mean square root value and human comfort by the riding value method. The results are shown in Table 1 [31].

Cui investigated the human comfort when the vehicle passed through the road-bridge transition section [32]. When the vehicle passed through the road-bridge transition

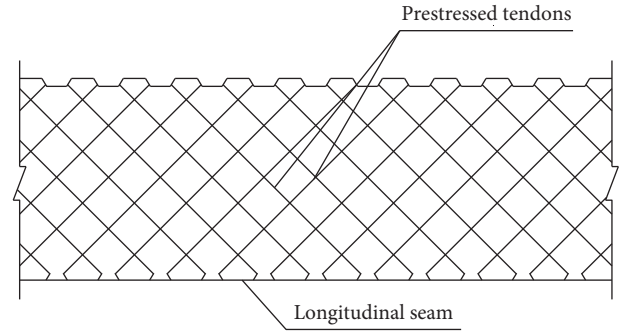

Figure 2: OPC schematic diagram.

section, it was easy to measure the mean square root value of vertical acceleration and weighted acceleration by installing the acceleration sensors on the vehicle. The vertical acceleration was tested when the vehicle passed through the road-bridge transition section at different speeds, and the weighted acceleration mean square root value of the human body was calculated by Fourier transform. The human body comfort in the transition section was determined according to the relationship between the driving comfort and weighted acceleration mean square root value in ISO2631-1-1997.

When the vehicle is running, it is in a vibrating state due to the road-bridge transition section unevenness. The vehicle vertical acceleration will cause the human body to feel uncomfortable. Therefore, in this study, acceleration sensors were installed in the vehicle to measure the vertical acceleration when the vehicle passed through the road-bridge transition section. The Fourier transform was used to obtain the weighted acceleration mean square root value of the human body.

Many types of vehicles with different models and performance parameters are seen on the road. The vibration transmitted by these different vehicles to the human body is also different. Automotive vehicles that pass through high-grade highways are mainly divided into passenger cars and trucks. In order to study the human body comfort when vehicle passed through the transition section, the bus Yutong ZK6119HB was selected as the testing vehicle, as shown in Figure 3. Table 2 shows the corresponding parameters of ZK6119HB.

3.1.2. Installation and Calibration of the Acceleration Sensor. The acceleration sensor was installed at the specified position. The acceleration signal was received by a piezoelectric acceleration sensor when the vehicle passed through the transition section. After the charge amplified, the charge signal was converted into a voltage signal, and then the acquisition card was used to achieve A/D conversion. In this paper, the A/D conversion is the conversion of analogy signal to digital signal, that is, the conversion of voltage signal to vertical acceleration. In addition, the data were stored through the software in the laptop. The connection diagram, physical diagram, and calibration system of the measuring system are shown in Figures 4–6.

Table 1: Relationship between weighted acceleration mean square root value and driving comfort.

Weighted acceleration mean square root value (m/s^2)	Human comfort
<0.315	Comfortable
0.315–0.63	Slightly uncomfortable
0.5–1	More slightly uncomfortable
0.8–1.6	Uncomfortable
1.25–2.5	Very uncomfortable
>2.0	Especially uncomfortable

Figure 3: Testing vehicle (Yutong ZK6119HB).

Table 2: Basic parameters.

Car model	Yutong ZK6119HB
Vehicle (length, width, height)	11290 mm, 2500 mm, 3580 mm
Maximum speed	115 km/h
Number of axes	2
Wheelbase	5550 mm
Number of seats	49 + 1 + 1
Minimum ground clearance	200 mm

3.1.3. Fixed Acceleration Sensor. In this test, the acceleration sensors were installed on the front seat and the bottom plate of testing vehicle. The acceleration sensors were fixed to ensure the accuracy of the test results and prevent it from falling from the floor or seat due to the vibration. The acceleration sensors were fixed on the metal plate by the magnets for the acceleration sensors base were made up of magnets, as shown in Figure 7.

In this test, two acceleration sensors were installed on the bottom of plate and seat. One was fixed on the chassis of vehicle and the vertical acceleration was measured when the vehicle passed through the transition section. The other was fixed on the front seat of vehicle and the vertical acceleration was measured when the vehicle passed through the transition section. A 300 W inverter was connected to a large battery, as shown in Figure 8. The charge amplifier had two wiring ports that could be connected to two acceleration sensors. In this work, the no. 1 line was connected to the front seat acceleration sensor and the no. 2 line was connected to the chassis acceleration sensor. The charge amplifier could be connected to a computer to collect data, as shown in Figure 9. The data collected by the computer existed in the form of time-domain signals. Finally, the acceleration absolute value was obtained by comparative analysis and calibration of the indoor test.

3.2. Transition Section Model. The void beneath cement pavement slab is a common phenomenon and it is distributed at the slab corner and seam edge, especially when the slab is long [33]. The model of AC + OPC composite structure was built using ANSYS. For the convenience of calculation, the following simplifications were made:

(1) Each layer was made of the continuous, isotropic linear elastic material

(2) The layers were completely continuous in the vertical direction, and no void appeared between the layers

(3) The pavement surface had the vertical uniform distribution load, and the displacement and stress at infinite depth and far away were all zero

(4) The elastic semispace foundation model was adopted in the analysis

The grid division used solid 45 units and the prestressed tendons were simulated by the space bar unit LINK 8. The load was the BZZ-100. The boundary conditions of model were as follows. (1) The base was taken as finite size for the convergence of analysis. (2) The bottom surface of the foundation was the fixed surface with complete restraint and the vertical surfaces around had the horizontal constraint. (3) The vertical surfaces around the base and asphalt layers had the horizontal constraint. The contact between the layers below base was completely smooth. (4) The four sides of the pavement slab were completely free boundaries. (5) No displacement was found in the X, Y, or Z direction of the bridge. (6) The contact unit simulation was used between the OPC slab and base and the friction coefficient was 0.8.

In the finite element model, the OPC slab had the length of 31.2 m and width of 5.4 m. The material parameters are shown in Table 3 and the finite element model of transition section is shown in Figure 10.

4. Results and Discussion

4.1. Control Criteria Based on Driving Comfort

4.1.1. Analysis of Driving Comfort. The differential settlement of short subgrade must be controlled in a certain range to improve the passengers' comfort. Two aspects of comfort and safety should be considered to obtain the permissible differential settlement. The permissible differential settlement for comfort is stricter than safety. As long as the differential settlement meets the comfort requirements, safety will certainly be satisfied.

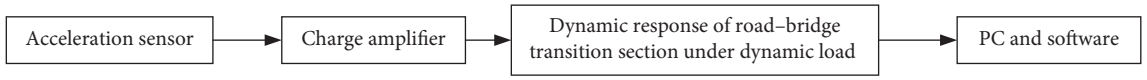

Figure 4: Connection diagram.

Figure 5: Physical diagram.

Figure 6: Calibration system.

(a) (b)

Figure 7: Fixed acceleration sensors. (a) The first test board. (b) The second test board.

The passenger's comfort is that passenger will not feel bump when passing through the transition section. The differential settlement control criteria of short subgrade were put forward by analyzing the differential settlement control indexes corresponding to different subjective feelings of the human body.

Zheng and Jing found the angle between the abutment and slab when the differential settlement occurred in the transition section. θ_1 was the angle before and after bridge pavement settlement. θ_2 was the angle between the bridge pavement and slab. Let $\theta = \theta_1 + \theta_2$ be the angle before and

Figure 8: Inverter and battery connection.

Figure 9: Data collection.

Table 3: Material parameters.

Structure	Thickness (d, cm)	Elasticity (E, MPa)	Poisson ratio (u)
Asphalt concrete	10	1200	0.25
OPC	24	31000	0.15
Cement-stabilized gravel	36	1800	0.2
Silty bed	700	40	0.35
Slope	700	40	0.35
Abutment	736	31000	0.15
Prestressed tendon	—	195000	0.3

after slab settlement and the tangent value (Δ) was the change value of longitudinal slope [34].

Figure 11 shows that the vehicle will vibrate when passing through the transition section. When the vehicle passes at a faster speed, the vibration will be relatively large. This will affect the driving comfort and safety. Taking the testing vehicle as an example, the excitation vibration effects of different speeds, different longitudinal slopes, and different slab lengths on the transition section were calculated.

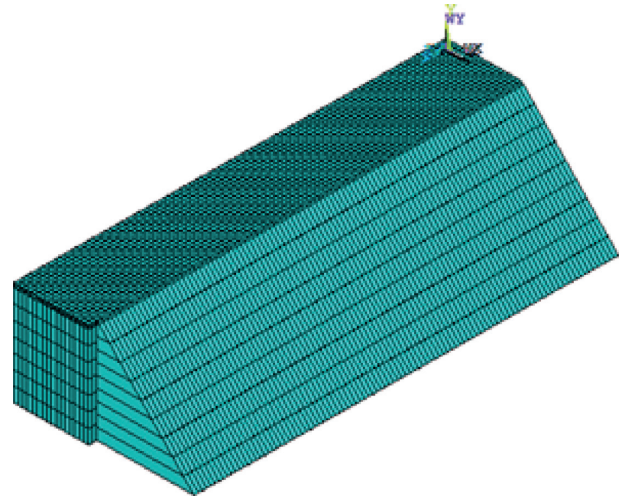

Figure 10: Finite element model of transition section.

In order to investigate the effects of speed, vertical slope, and slab length on the vertical acceleration, the single factor experiment was conducted in this paper. The interaction effects of changing two or more of these parameters simultaneously will be incorporated into our future research.

The slab length was unified to 8 m. The wheelbase was 4.7 m. The calculated speed was 60 km/h, 80 km/h, 100 km/h, and 120 km/h, respectively. The relationship between the vehicle acceleration and speed is shown in Figure 12.

Figure 12 shows that the vertical acceleration increases significantly with the speed increase. Compared with no slab, the vertical acceleration value and bump are significantly reduced. Therefore, setting up of slab in the transition section is very necessary.

When the slab length was 8 m and the speed was 100 km/h, the vertical slope was 0.2%, 0.4%, 0.6%, 0.8%, and 1.0%, respectively. The change of vertical acceleration is shown in Figure 13.

Figure 13 reveals that the vertical acceleration increases significantly with the longitudinal slope increase. This indicates that the longitudinal slope is a sensitive factor that affected the vehicle vibration.

When the speed was unified at 100 km/h, the wheelbase was 4.7 m and the longitudinal slope was 0.5%. The slab length was 6 m, 8 m, 10 m, and 12 m, respectively. The relationship between the vertical acceleration and different slab lengths is shown in Figure 14.

Figure 14 shows that the effect of slab length on the vertical acceleration is not significant when the slab length is changed from 6 m to 12 m. Due to the limitation of experimental conditions, other experiments in which the slab length is greater than 12 m have not been done, and this will be conducted in our further research. From the theoretical perspective, the slope difference between the bridge pavement and slab causes the vehicle to vibrate near the abutment. However, the influence of slope difference on the vehicle vibration gradually decreases with the slab length increase. The long slab will reduce the change value of longitudinal slope, which is beneficial to reduce vibration.

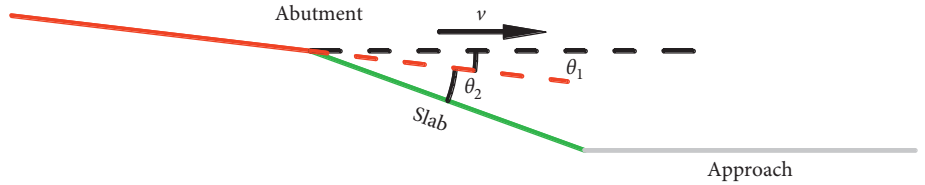

Figure 11: Transition section model when slabs are installed.

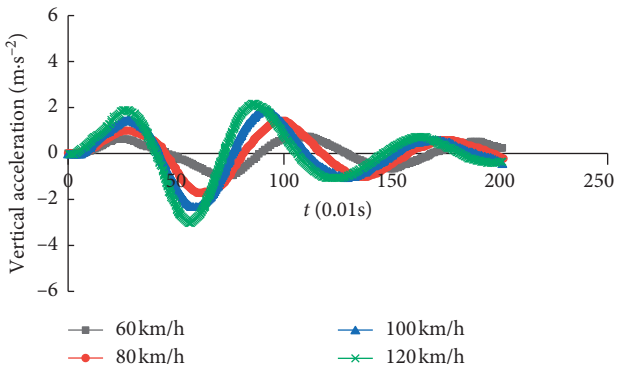

Figure 12: Vertical acceleration of testing vehicle at different speeds.

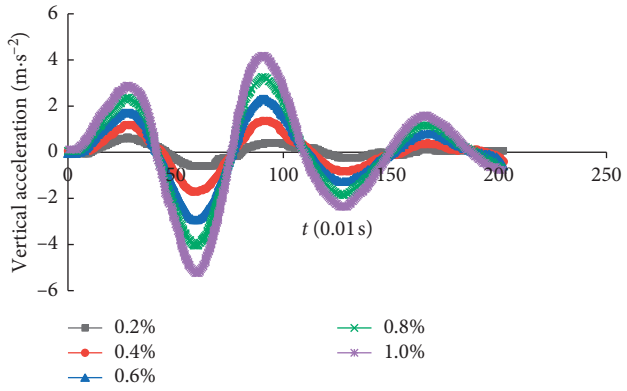

Figure 13: Vertical acceleration of testing vehicle at different longitudinal slopes.

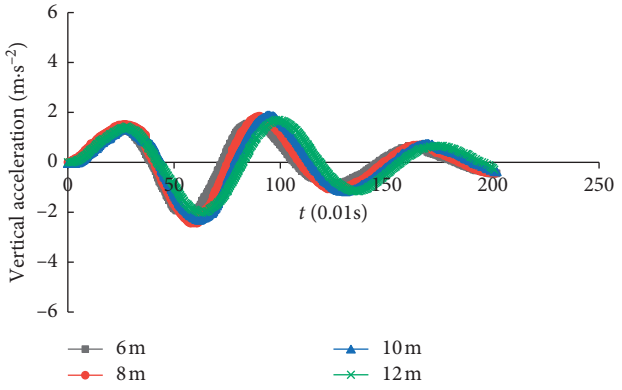

Figure 14: Vertical acceleration of testing vehicle at different slab lengths.

The aforementioned analysis shows that the setting up of transition section between the road and bridge is essential to reduce the vehicle vibration. The transition section plays a vital role in reducing the vehicle vibration by increasing the slab length and limiting the differential settlement. The passenger's comfort is improved with the slab length increase. By replacing the slab with AC + OPC composite pavement in the short subgrade, the transition section distance can be effectively increased, which has a positive impact on easing vehicle vibration and improving the driving comfort.

Figures 12–14 reveal that the vertical acceleration of vehicle caused by the vibration tends to be steady within 2 s. When passing through the transition section within 2 s at speeds of 60 km/h, 80 km/h, 100 km/h, and 120 km/h, the required distances of transition section are 33 m, 44 m, 55 m, and 66 m, respectively. Due to the linearity limitation at the short subgrade, the speed at the transition section is often limited. The vehicle speed can be as high as 100 km/h. When the vehicle passes through the transition section, the vertical acceleration of vehicle is not felt when the slab length is 55 m. However, the length of short subgrade is not all greater than 55 m for the limitation of terrain and requirements of linearity design. In order to ensure the driving comfort, the differential settlement must be controlled within a certain range.

4.1.2. Establishment of Control Criteria Based on Driving Comfort. In this study, the control criteria for differential settlement of short subgrades with different lengths are proposed based on the driving comfort:

(1) When the length (L) of short subgrade is less than 8 m ($L \leq 8$ m), the slab is set up at the short subgrade and setting up of AC + OPC composite pavement is not required. The control criteria of differential settlement are implemented in accordance with Table 4 obtained according to the research results of our research group.

(2) When 8 m $\leq L \leq$ 30 m and the AC + OPC composite pavement is applied at the short subgrade, the mean value of the upper and lower maximum longitudinal slope value in Table 4 is taken as the maximum allowable longitudinal slope difference (Δ_2). The results of allowable differential settlement at each speed in the end of the AC + OPC composite pavement far from abutment are summarized in Table 5.

Table 4: Values of longitudinal slope and settlement of transition section corresponding to different speeds in "slightly uncomfortable" state.

Speed (km/h)	Maximum longitudinal slope value (%)	Maximum settlement value (cm)
60	0.19–0.80	1.5–5.1
80	0.19–0.74	1.5–4.4
100	0.19–0.60	1.5–4.0
120	0.19–0.46	1.5–3.4

Table 5: Control criteria for differential settlement of short subgrade at different speeds when $8\,\text{m} < L \leq 30\,\text{m}$.

Speed (km/h)	Δ_1 (%)	Δ_2 (%)	Δ (%)	Maximum settlement value (cm)
60	0.2	0.49	0.69	5.5~20.7
80	0.2	0.46	0.66	5.3~19.8
100	0.2	0.39	0.59	4.7~16.8
120	0.2	0.32	0.52	4.2~15.6

Δ_1 = the longitudinal slope difference of bridge pavement. Δ_2 = the maximum allowable longitudinal slope difference of slab. Δ = the maximum allowable longitudinal slope difference of bridge pavement and slab.

(3) When $30\,\text{m} \leq L \leq 55\,\text{m}$, the differential settlement tends to be stabilized by 30 m transition. When the length is more than 30 m, the ability to adapt to the differential settlement improves with the length of AC + OPC composite pavement increases. The maximum allowable longitudinal slope difference at different speeds corresponding to the application of the AC + OPC composite pavement at the short subgrade should be reduced on the basis of Table 5. When the length of short subgrade is greater than 30 m, the settlement is basically the same. When the length of short subgrade is 55 m, the longitudinal slope difference is 30/55 of the original according to the geometric relationship. The results of allowable differential settlement at each speed in the end of the AC + OPC composite pavement far from abutment are summarized in Table 6.

(4) When the length of short subgrade is greater than 55 m, the differential settlement between the OPC slab and abutment reaches the maximum value. This situation is almost impossible to achieve in practice. Due to the long length of OPC slab, the void beneath slab occurred. When the length of short subgrade is greater than 55 m, the differential settlement is controlled according to the control criteria based on the void area beneath cement pavement slab. It will be discussed in the following section.

4.2. Control Criteria Based on the Void Area beneath the Slab. The situation is different for the different lengths of short subgrade. The void beneath slab will occur for the long length of OPC slab. In order to obtain the control criteria based on the void area beneath slab, the stress and void area beneath slab should be studied firstly. However, the stress and void area beneath slab are hard to be measured. The relationships between the stress and deflection and the void area beneath slab and deflection were established for the reason that the deflection is easily measured.

Table 6: Control criteria for differential settlement of short subgrade at different speeds when $30\,\text{m} < L \leq 55\,\text{m}$.

Speed (km/h)	Δ_1 (%)	Δ_2 (%)	Δ (%)	Maximum settlement value (cm)
60	0.2	0.27	0.47	14.1~25.8
80	0.2	0.25	0.45	13.5~24.7
100	0.2	0.21	0.41	12.3~22.5
120	0.2	0.17	0.37	11.1~20.3

4.2.1. Influence of Layer Parameters on Stress and Deflection. The color-coded deformation plots in the middle of longitudinal seam edge and at the slab corner are shown in Figure 15. The influence of different layer parameters on stress and deflection are shown in Figure 16.

Figure 16(a) reveals that the influence of asphalt layer thickness on the stress and deflection is not significant. When the asphalt layer thickness increases from 4 cm to 16 cm, the deflection increases by 5.3%. Furthermore, the flexural stress at the bottom of OPC layer, the shear stress, and tensile stress at the bottom of asphalt layer and the flexural stress at the bottom of base layer reduce by 2.6%, 6%, 31.4%, and 1.8%, respectively. The increase of asphalt layer thickness is conducive to dispersion and reduction of the load stress and reduction of the stress at the bottom of OPC layer. However, the asphalt layer in the AC + OPC composite pavement mainly plays functional role in protecting the OPC layer, reducing noise, improving driving comfort, and so on. It is not realistic to greatly reduce the OPC layer stress by increasing the asphalt layer thickness. Figure 16(b) shows that the effect of the asphalt layer modulus on deflection is significant. When the asphalt layer modulus changes from 600 MPa to 1800 MPa, the deflection reduces by 12.7%. The flexural stresses at the bottom of OPC slab and base layer gradually decrease and the rest are basically unchanged.

Figure 16(c) reveals that the shear stress of asphalt layer and the flexural stress of OPC layer increase with the OPC modulus increase, increasing by 12.4% and 19.9%, respectively. The deflection and flexural stress at the bottom of base layer reduce by 7% and 11%, respectively. Figure 16(d) illustrates that the OPC layer thickness has a great influence on the stress and deflection. When the OPC layer thickness increases from 16 cm to 28 cm, the flexural stress at the bottom of OPC layer, deflection, maximum shear stress and tensile stress of asphalt layer, and flexural stress at the bottom of base layer reduce by 47.4%, 24.3%, 50.2%, 18.5%, and 37.6%, respectively. The aforementioned analysis shows that the OPC layer thickness had a great influence on the stress, and the increase in OPC layer thickness can effectively reduce the stress.

Figure 16(e) shows that the influences of base layer modulus on the flexural stress at the bottom of base layer and OPC layer are significant. When the base layer modulus

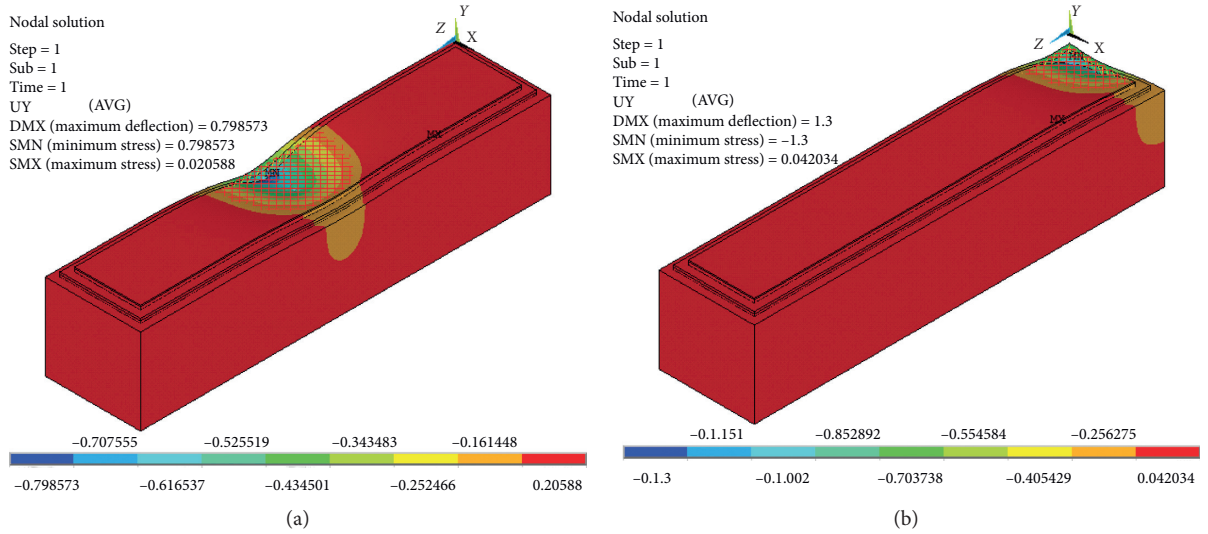

Figure 15: Color-coded deformation plots. (a) The middle of longitudinal seam edge. (b) The slab corners.

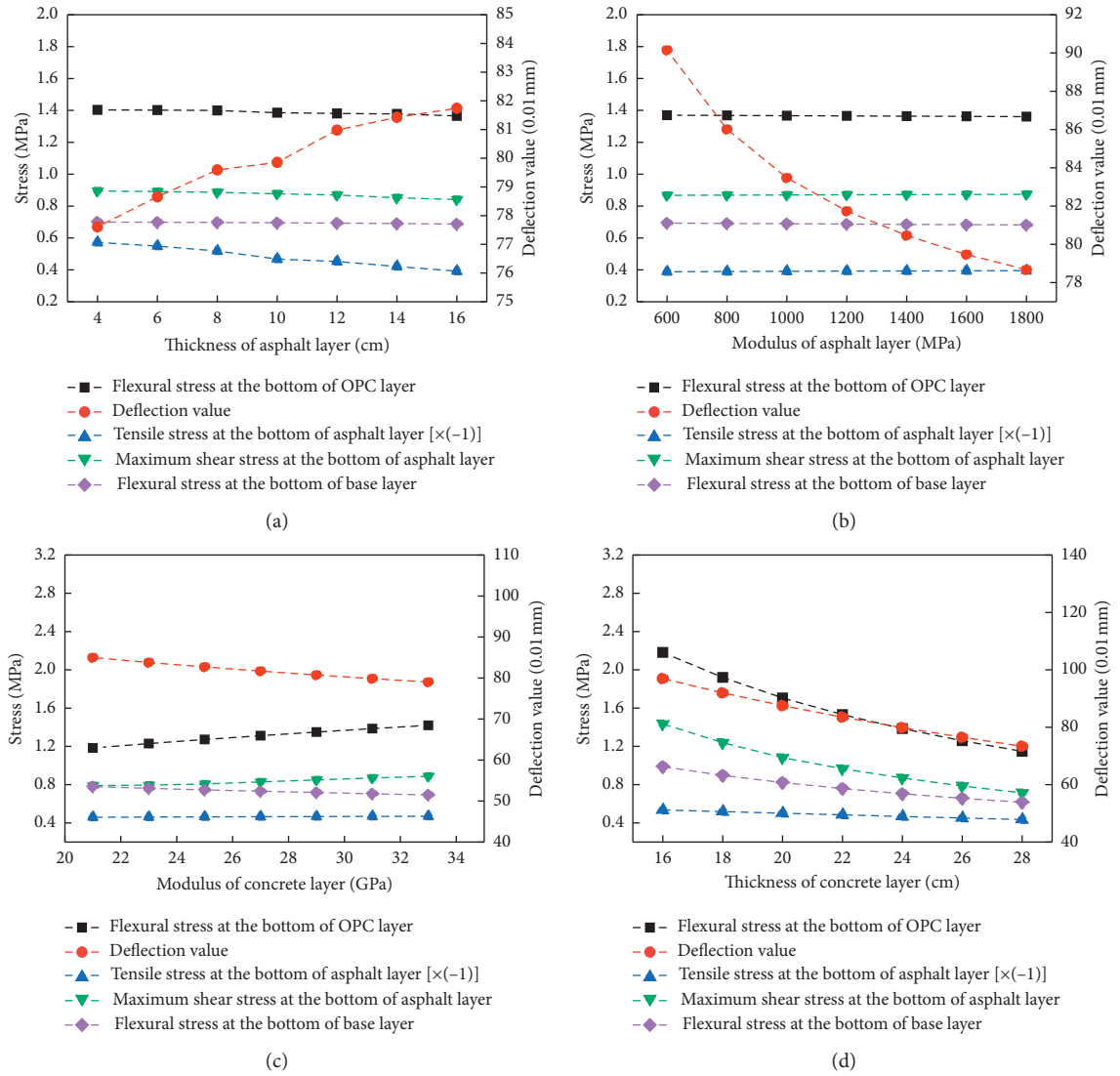

Figure 16: Continued.

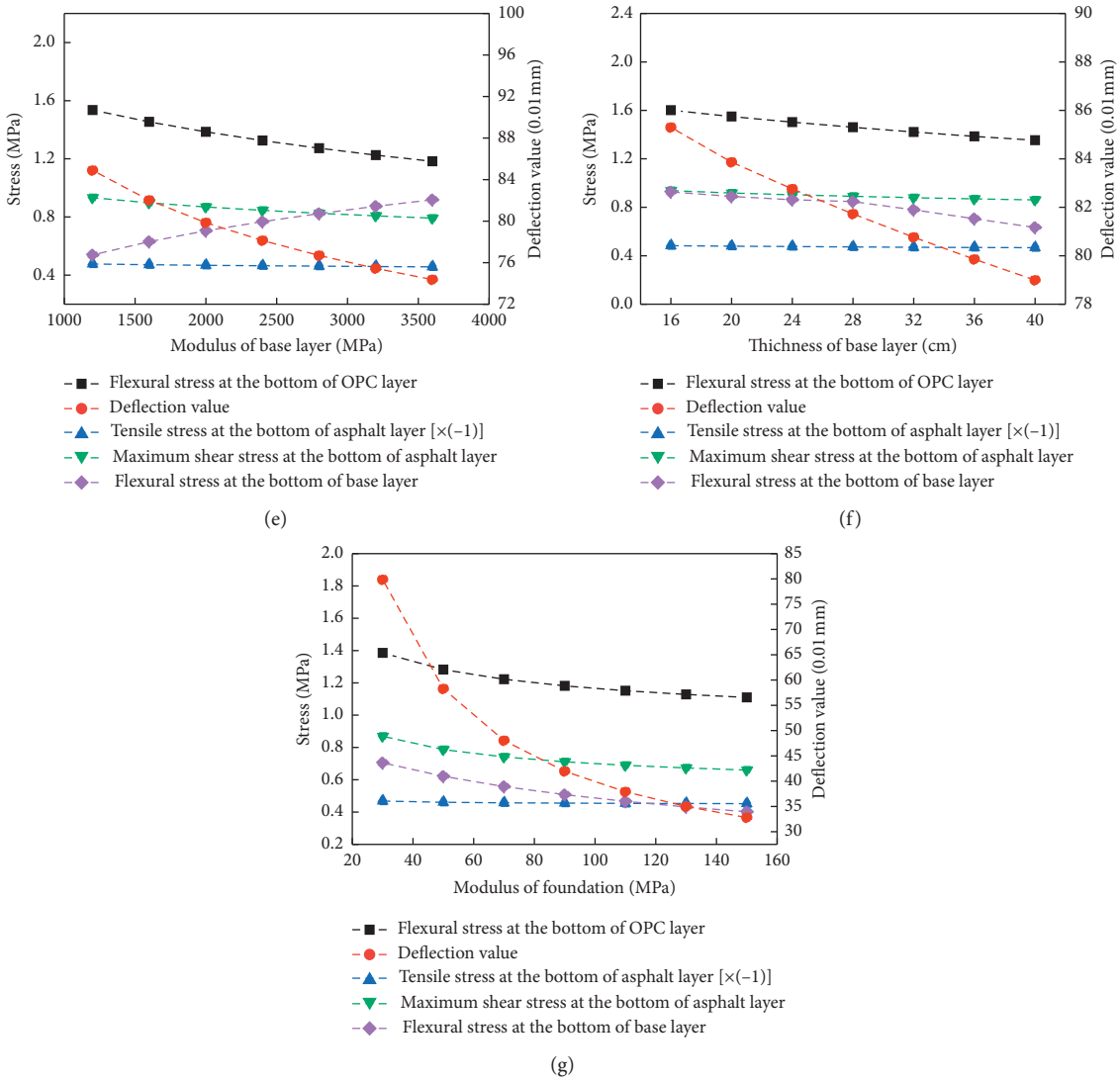

Figure 16: Influence of different layer parameters on stress and deflection. (a) Asphalt layer thickness. (b) Asphalt layer modulus. (c) OPC modulus. (d) OPC thickness. (e) Base layer modulus. (f) Base layer thickness. (g) Foundation modulus.

increases from 1200 MPa to 3600 MPa, the flexural stress at the bottom of base layer increases by 70.5%, and the flexural stress and deflection of OPC layer reduce by 23% and 12%, respectively. The base layer modulus has little effects on the tensile and shear stress at the bottom of asphalt layer. Figure 16(f) shows that the indexes of pavement structure have a decreasing trend, and the reduction of flexural stress at the bottom of base layer is remarkable with the base layer thickness increase. When the base layer thickness increases from 16 cm to 40 cm, the flexural stress at the bottom of base and OPC layer and deflection reduce by 23.9%, 13.5%, and 6.4%, respectively. The tensile and shear stress at the bottom of asphalt layer is not reduced significantly.

Figure 16(g) reveals that the flexural stress at the bottom of base and OPC layer and deflection reduce by 42.9%, 19.9%, and 58.9%, respectively, with the foundation modulus increase. The tensile and maximum shear stress at the bottom of asphalt layer is not changed significantly. Therefore, good foundation conditions are very important in the design of pavement structure to prevent excessive stress and deflection on the OPC layer.

Based on the above analysis, the asphalt layer modulus, OPC layer thickness and modulus, base layer thickness and modulus, and foundation modulus have a significant effect on the flexural stress and deflection, especially the OPC layer thickness. In order to extend the pavement life, the void area beneath cement pavement slab should be controlled within a certain range.

4.2.2. Identification of Void Area beneath the Slab. The relationship between the deflection and void area beneath slab in the middle of the longitudinal seam edge and at the slab corner is shown in Figure 17.

The deflections in the middle of longitudinal seam edge and at the slab corner are obtained by changing the void area beneath slab in the finite element model. Figure 17(a) shows a good relationship between the void area beneath slab A_{ZZ}

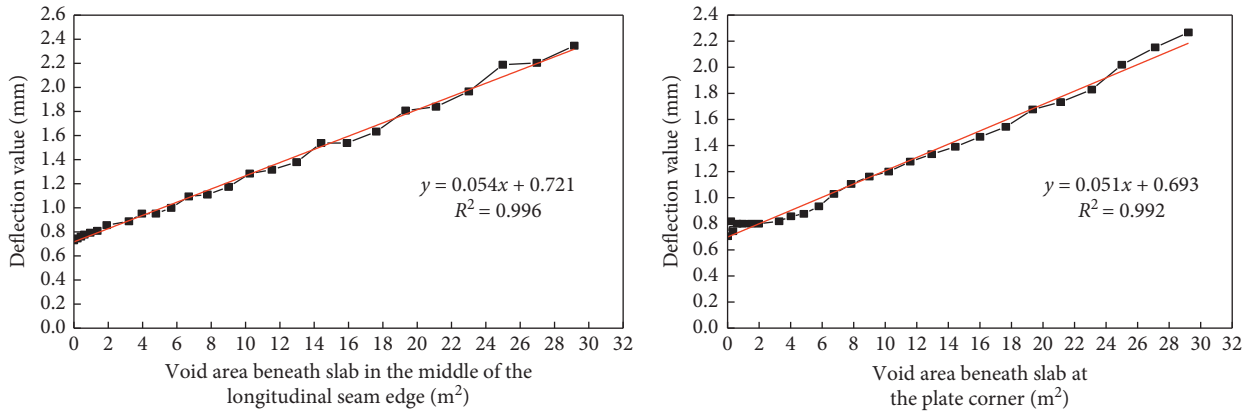

FIGURE 17: Relationship between the deflection and void area beneath slab. (a) The middle of longitudinal seam edge. (b) The slab corners.

(m^2) and deflection l (mm) in the middle of longitudinal seam edge. After processing and fitting, the relationship between l and A_{ZZ} is obtained as follows:

$$l = 0.054A_{zz} + 0.721, \tag{1}$$

where l and A_{zz} are the deflection and void area beneath slab in the middle of longitudinal seam edge, respectively.

Figure 17(b) shows that the void area beneath slab A_{bj} (m^2) and deflection l (mm) has a good relationship at the slab corner. After processing and fitting, the relationship between l and A_{bj} is obtained as follows:

$$l = 0.051A_{bj} + 0.693, \tag{2}$$

where l and A_{bj} are the deflection and void area beneath slab at the slab corner, respectively.

In practice, the measured deflection is put into (1) and (2) to obtain the void area beneath slab of the corresponding position.

4.2.3. Relationship between the Additional Stress and Void Area beneath the Slab. Under the same load action, the stress generated at the same position under the situation of void beneath cement pavement slab is greater than that not void, which is the additional stress [35]. In this paper, the additional flexural stress at the bottom of OPC slab in the middle of longitudinal seam edge and slab corner was investigated.

The relationship between the additional flexural stress and void area beneath slab in the middle of the longitudinal seam edge and at the slab corner is shown in Figure 18.

Figure 18(a) shows that the additional flexural stress at the bottom of the OPC slab increases with the void area beneath slab increase. The relationship between σ_{zzf} (MPa) and A_{zz} (m^2) is obtained after processing and fitting as follows:

$$\sigma_{zzf} = (0.38763 \pm 0.07027)A_{zz}^{(0.45456 \pm 0.04426)} + 0.07937, \tag{3}$$

where σ_{zzf} is the additional flexural stress at the bottom of OPC slab in the middle of longitudinal seam edge. A_{zz} is the void area beneath slab in the middle of longitudinal seam edge.

Figure 18(b) shows that the additional flexural stress at the bottom of the OPC slab increases with the void area beneath slab increase. The relationship between σ_{bij} (MPa) and A_{bj} (m^2) is obtained after processing and fitting as follows:

$$\sigma_{bij} = (0.45499 \pm 0.09155)A_{bj}^{(0.42263 \pm 0.04629)} + 0.10539. \tag{4}$$

where σ_{bij} is the additional flexural stress at the bottom of OPC slab at the slab corner. A_{bj} is the void area beneath slab at the slab corner.

4.2.4. Establishment of Control Criteria Based on Void Area beneath the Slab. The allowable additional flexural stress is determined by the combined effects of load stress, temperature fatigue stress, and additional stress as the following formula:

$$\gamma_r\left(\sigma_{pr} + \sigma_{tr}\right) + \sigma_f + \sigma_F \le f_r, \tag{5}$$

where σ_{pr} is the load fatigue stress (MPa) generated at the critical load position calculated by (6). σ_{tr} is the temperature gradient fatigue stress (MPa) generated at the critical load position calculated by (10). σ_f and σ_F are the additional flexural stress and frictional stress, respectively, in MPa. γ_r is the reliability factor. f_r is the standard value of flexural stress of cement concrete, in MPa.

(1) Load Fatigue Stress. The load fatigue stress in the critical load position is calculated using

$$\sigma_{pr} = k_r k_f k_c \sigma_{ps}, \tag{6}$$

where k_r is the stress reduction coefficient. k_f is the fatigue stress coefficient. k_c is the comprehensive coefficient that is determined according to the highway grade. σ_{ps} is the load

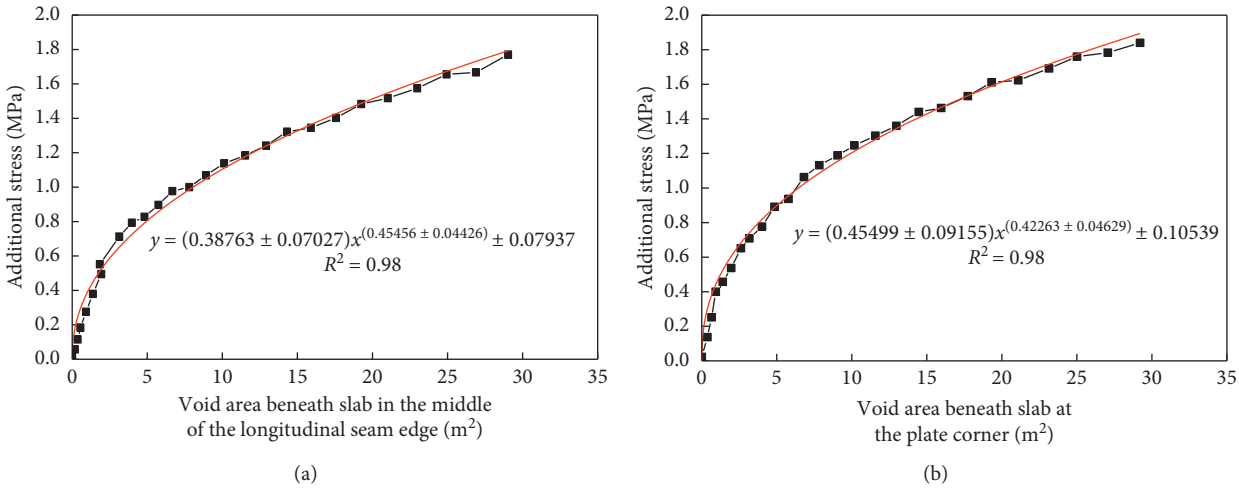

FIGURE 18: Relationship between the additional flexural stress and void area beneath slab. (a) The middle of longitudinal seam edge. (b) The slab corners.

stress obtained from the design load at the critical load position, and it is calculated using

$$\sigma_{ps} = P \times \left(1.7340 \times 10^{-5} E_2 + 7.9346 \times 10^{-5} h_1^2 - 5.9006 \times 10^{-5} h_1 h_2 + 3.3087 \times 10^{-5} h_2^2 - 5.9614 \times 10^{-7} h_2 E_2 - 3.8060 \times 10^{-16} h_2 E_1 E_2^2 - 5.1532 \times 10^{-8} E_2 E_3 + 3.7582 \times 10^{-7} E_3^2 - 0.0024q\right), \quad (7)$$

where E_1, E_2, and E_3 are the modulus of OPC slab, subgrade, and foundation, respectively, in MPa. h_1 and h_2 are the thickness of asphalt layer and OPC slab, in mm. q is the prestress, in MPa. P is the standard axle load (100 kN).

The load fatigue coefficient is calculated using (8) during the design period:

$$k_f = N_e^{\lambda}, \quad (8)$$

where N_e is the number of cumulative effects on the axis during the design period. λ is the material fatigue index ($\lambda = 0.057$).

(2) Temperature Fatigue Stress. The temperature fatigue stress generated at the critical position is calculated using

$$\sigma_{tr} = k_t \sigma_{t,\max}, \quad (9)$$

where k_t is the temperature fatigue stress coefficient considering the cumulative fatigue effect of the temperature stress. $\sigma_{t,\max}$ is the maximum temperature stress calculated according to

$$\sigma_{t,\max} = T_g^{0.5266}\left(5.9345 \times 10^{-5} E_1 + 1.0091 \times 10^{-7} E_2^2 + 0.0008 h_1 h_2 + 5.1842 \times 10^{-6} h_2 E_1 + 0.1646q + 5.9854u - 0.2793u h_2\right), \quad (10)$$

where μ is the friction coefficient of sliding layer. T_g is temperature gradient (°C · cm).

(3) Frictional Stress. The friction stress is calculated using

$$\sigma_F = u_r \rho x, \quad (11)$$

where u_r is the friction coefficient at the bottom of slab. ρ is the concrete density. x is the distance between the location of calculating load and slab end. It is advisable to take half the length of the slab.

The additional flexural stress obtained by (5) is substituted into (3) or (4) according to the location, and the maximum void area beneath slab at the corresponding position will be obtained.

The control criteria for differential settlement of short subgrade with different lengths are proposed based on the driving comfort and void area beneath slab. In the construction of short subgrade, the filling process and criteria can be reasonably selected according to the speed standard, the length of short subgrade, and the aforementioned differential settlement control criteria. When the differential settlement of short subgrade leads to the failure of any of the aforementioned aspects, it is necessary to take measures such as grouting at the bottom of the slab to treat the differential settlement.

5. Conclusions

This study presented the definition of short subgrade based on the comfort principle and related research results; then the advantages and applicability of AC + OPC composite pavement were introduced. The driving comfort was investigated and the control criteria for differential settlement of short subgrade with different lengths based on the driving comfort were obtained. In addition, the influence of different layer parameters on stress and deflection and the control criteria for differential settlement of short subgrade based on

the void area beneath slab were obtained using the finite element software:

(1) The asphalt layer thickness only has a great influence on the flexural stress at the bottom of asphalt layer, while the influence on the other indexes of the pavement structure is not significant. When the asphalt layer modulus changes from 600 MPa to 1800 MPa, the deflection reduces by 12.7%. The asphalt layer modulus has little effects on the other indexes. When the OPC layer modulus increases, the increases in the shear stress of asphalt layer and the flexural stress at the bottom of OPC layer are significant. Therefore, the OPC layer modulus should not be too large. It can cause excessive flexural and tensile stress at the bottom of OPC layer to damage the structure and cause shear failure. When the OPC layer thickness is increased from 16 cm to 28 cm, the flexural stress at the bottom of OPC layer reduces by 47.4%. The increase of OPC layer thickness can effectively improve the stress of pavement structure. Therefore, the economics and stress should be comprehensively considered when determining the OPC layer thickness.

(2) The control criteria for differential settlement of short subgrade with different lengths based on driving comfort and void area beneath slab are obtained as follows.

The control criteria for differential settlement of short subgrade with different lengths ($L \leq 8$ m, 8 m $< L \leq 30$ m, and 30 m $< L \leq 55$ m) are proposed according to the 2 s stroke and driving comfort of different speeds (60 km/h, 80 km/h, and 100 km/h). When L > 55 m, the control criteria based on void area beneath slab are employed.

Data Availability

The data used to support the findings of this study are included within the article.

Conflicts of Interest

The authors declare that there are no conflicts of interest regarding the publication of this paper.

Acknowledgments

This research was funded by the Fundamental Research Funds for the Central Universities (Grant no. 310821163502), Transportation Science and Technology Project of Shaanxi Province (Grant no. 13–04K), and the Transportation Department of Shandong Province (Grant no. Lujiaokeji [2017] 28).

References

[1] C. Cai, G. Z. Voyiadjis, and X. Shi, "Determination of interaction between bridge concrete approach slab and embankment settlement (final report)," Louisiana Transportation Research Center (LTRC), Louisiana Department of Transportation and Development (LADOTD), 150, Report No. FHWA/LA.05/, Baton Rouge, LA, USA, 2005.

[2] B. Dupont and D. L. Allen, "Movement and settlements of highway bridge approaches (final report)," Kentucky Transportation Cabinet, 74, Report No. KTC-02e18/SPR-220-00-IF, Frankfort, KY, USA, 2005.

[3] L. R. Lenke, "Settlement issues-bridge approach slabs (final report)," Report No. NM04MNT-02, New Mexico Department of Transportation, Albuquerque, NM, USA, 2005.

[4] J. H. Long, S. M. Olson, T. D. Stark, and E. A. Samara, "Differential movement at embankment-bridge structure interface in Illinois," *Transportation Research Record: Journal of the Transportation Research Board*, vol. 1633, no. 1, pp. 53–60, 1998.

[5] X. Q. Zhu and S. S. Law, "Dynamic load on continuous multilane bridge deck from moving vehicles," *Journal of Sound and Vibration*, vol. 251, no. 4, pp. 697–716, 2002.

[6] F. Niu, Z. Lin, J. Lu, H. Liu, and Z.-Y. Xu, "Characteristics of roadbed settlement in embankment-bridge transition section along the Qinghai-Tibet railway in permafrost regions," *Cold Regions Science and Technology*, vol. 65, no. 3, pp. 437–445, 2011.

[7] V. Pakrashi, A. O'Connor, and B. Basu, "A bridge-vehicle interaction based experimental investigation of damage evolution," *Structural Health Monitoring: An International Journal*, vol. 9, no. 4, pp. 285–296, 2010.

[8] N. Zhang and H. Xia, "Dynamic analysis of coupled vehicle-bridge system based on inter-system iteration method," *Computers & Structures*, vol. 114-115, pp. 26–34, 2013.

[9] S. Ahmari, M. Yang, and H. Zhong, "Dynamic interaction between vehicle and bridge deck subjected to support settlement," *Engineering Structures*, vol. 84, pp. 172–183, 2015.

[10] Y. Cao and J. Qu, "Influence of subgrade differential settlement on riding performance of high-speed train," In J. Pombo and G. Jing (eds) Recent Developments in Railway Track and Transportation Engineering, GeoMEast 2017, Sustainable Civil Infrastructures, Springer, Cham, Switzerland, pp. 121–132, 2018.

[11] A. Paixão, E. Fortunato, and R. Calçada, "The effect of differential settlements on the dynamic response of the train-track system: a numerical study," *Engineering Structures*, vol. 88, pp. 216–224, 2015.

[12] J. C. O. Nielsen and X. Li, "Railway track geometry degradation due to differential settlement of ballast/subgrade-numerical prediction by an iterative procedure," *Journal of Sound and Vibration*, vol. 412, pp. 441–456, 2018.

[13] H. Jiang, X. Li, G. Xin, Z. Yao, J. Zhang, and M. Liang, "Geometry mapping and additional stresses of ballastless track structure caused by subgrade differential settlement under self-weight loads in high-speed railways," *Transportation Geotechnics*, vol. 18, pp. 103–110, 2019.

[14] Y. Guo and W. Zhai, "Long-term prediction of track geometry degradation in high-speed vehicle-ballastless track system due to differential subgrade settlement," *Soil Dynamics and Earthquake Engineering*, vol. 113, pp. 1–11, 2018.

[15] M. Rith, Y. K. Kim, and S. W. Lee, "Behavior of RCC-base composite pavement for heavy duty area," *Construction and Building Materials*, vol. 175, pp. 144–151, 2018.

[16] M. Rith, Y. K. Kim, S. J. Hong, and S. W. Lee, "Effect of horizontal loading on RCC-base composite pavement performance at heavy duty area," *Construction and Building Materials*, vol. 131, pp. 741–745, 2017.

[17] M. S. Luther, *Mechanistic Investigation of Reflection Cracking of Asphalt Overlays*, Committee on Design of Composite

Pavement and Structural Overlays, Charlottesville, VA, USA, 1976.

[18] B. F. McCullough, *Three-Dimensional Nonlinear Finite Element Analysis of Continuously Reinforced Concrete Pavements*, The University of Texas at Austin, Austin, TX, USA, 2000.

[19] J. L. Robinson and R. Luna, *Deformation Analysis of Modelling of Missouri Bridge Approach Embankments*, ACE Geotechnical Special Publication, Hayti, MO, USA, 2004.

[20] S. H. Chew, H. L. Phoon, K. H. Loke et al., "Geotextile reinforced piled embankment for highway bridges," in *Proceedings of the Eighth International Conference on Applications of Advanced Technologies in Transportation Engineering*, pp. 438–443, Beijing, China, May 2004.

[21] X. M. Shi, C. S. Cai, G. Voyiadjis, and Z. Zhang, "Finite element analysis of concrete approach slab on soil embankment," in *Proceedings of the Geotechnical Engineering for Transportation Projects*, pp. 393–402, Los Angeles, CA, USA, July 2004.

[22] W. J. Yu, "Discussion on early disease and prevention of expressway," *Journal of Highway and Transportation Research and Development*, vol. 17, no. 6, pp. 10–14, 2000.

[23] Y. L. Wang, "Discussion on the treatment of bridgehead jumping in soft soil foundation," *Journal of Highway and Transportation Research and Development*, vol. 17, no. 1, pp. 28–30, 2000.

[24] Y. T. Ding, "Discussion on the causes and prevention of highway bridge head jumping," *Journal of Highway and Transportation Research and Development*, vol. 19, no. 5, pp. 92–98, 2002.

[25] Jianji, No. 97, Supplementary Provisions to Improve the Railway Subgrade Engineering Design and Quality, 2003, https://wenku.baidu.com/view/f51ecc69561252d380eb6eff.html.

[26] Department of Transport of Shaanxi Province, *Main Points of Quality Work of Highway Construction Engineering in Shaanxi Province*, Department of Transport of Shaanxi Province, Shaanxi, China, 2009.

[27] X. D. Pan, *The Application of Body Information Technology on Safety Evaluation of Road Alignment*, Tongji University, Shanghai, China, 2002.

[28] D. S. Zhang, S. Han, W. W. Han et al., "Research on key design parameters of two direction cross-tensioned prestressed cement concrete pavement," *Highway*, vol. 11, pp. 70–73, 2010.

[29] W. W. Han, *Study on the Design and Application of Cross-Tensioned Prestressed Concrete Pavement*, Chang'an University, Xi'an, China, 2010.

[30] X. Zheng, "Measurement and evaluation of automobile vibration comfort," *Bus & Coach Technology and Research*, vol. 4, pp. 9–18, 2000.

[31] ISO2631-1997, *Mechanical Vibration and Impact-Evaluation of Human Exposure to Whole-Body Vibration-Part 1: General Requirement*, International Organization for Standardization, Geneva, Switzerland, 1997.

[32] M. X. Cui, *Control Standard for Differential Settlement in Bridge-Subgrade Transition Section Based on Comfort Property*, Chang'an University, Xi'an, China, 2010.

[33] B. Zhang, H. Zhao, Y. H. Zhong et al., "Analysis method of angular-emptying area of cement concrete pavement based on deflection ratio," *Journal of china & Foreign Highway*, vol. 30, no. 5, pp. 83–86, 2010.

[34] W. Jing, *Research on Dynamic Response of Vehicle-Pavement in the Bridge-Subgrade Transition Section Base on Safety*, Chang'an University, Xi'an, China, 2010.

[35] H. Zhang, J. M. Ling, J. Yuan et al., "Theory analysis of cement concrete pavement structure based on existence of disengaging under slab," *Journal of Tongji University (Natural Science)*, vol. 40, no. 11, pp. 1677–1679, 2012.